(4)

AD-A219 784

RADC-TR-89-357
Final Technical Report
February 1990

ADVANCED GUIDED WAVE ELECTRO-OPTICAL SWITCHES

Texas A&M University

O. Eknoyan and H.F. Taylor

This effort was funded totally by the Laboratory Director's Fund.

APPROVED FOR PUBLIC RELEASE; DISTRIBUTION UNLIMITED

Rome Air Development Center
Air Force Systems Command
Griffiss Air Force Base, NY 13441-5700

This report has been reviewed by the RADC Public Affairs Division (PA) and is releasable to the National Technical Information Service (NTIS). At NTIS it will be releasable to the general public, including foreign nations.

RADC-TR-89-357 has been reviewed and is approved for publication.

APPROVED: Richard A Soref

RICHARD A. SOREF
Project Engineer

APPROVED: Harold Roth

HAROLD ROTH
Director of Solid State Sciences

FOR THE COMMANDER:

BILLY G. OAKS
Directorate of Plans & Programs

If your address has changed or if you wish to be removed from the RADC mailing list, or if the addressee is no longer employed by your organization, please notify RADC (ESOC) Hanscom AFB MA 01731-5000. This will assist us in maintaining a current mailing list.

Do not return copies of this report unless contractual obligations or notices on a specific document require that it be returned.

UNCLASSIFIED
SECURITY CLASSIFICATION OF THIS PAGE

REPORT DOCUMENTATION PAGE

Form Approved OMB No. 0704-0188

1a. REPORT SECURITY CLASSIFICATION UNCLASSIFIED	1b. RESTRICTIVE MARKINGS N/A
2a. SECURITY CLASSIFICATION AUTHORITY N/A	3. DISTRIBUTION/AVAILABILITY OF REPORT Approved for public release; distribution unlimited.
2b. DECLASSIFICATION/DOWNGRADING SCHEDULE N/A	
4. PERFORMING ORGANIZATION REPORT NUMBER(S) N/A	5. MONITORING ORGANIZATION REPORT NUMBER(S) RADC-TR-89-357
6a. NAME OF PERFORMING ORGANIZATION Texas A & M University 6b. OFFICE SYMBOL (If applicable)	7a. NAME OF MONITORING ORGANIZATION Rome Air Development Center (ESOC)
6c. ADDRESS (City, State, and ZIP Code) Electrical Engineering Department College Station TX 77840-3128	7b. ADDRESS (City, State, and ZIP Code) Hanscom AFB MA 01731-5000
8a. NAME OF FUNDING/SPONSORING ORGANIZATION Rome Air Development Center 8b. OFFICE SYMBOL (If applicable) ESOC	9 PROCUREMENT INSTRUMENT IDENTIFICATION NUMBER F19628-87-K-0027
8c. ADDRESS (City, State, and ZIP Code) Hanscom AFB MA 01731-5000	10. SOURCE OF FUNDING NUMBERS PROGRAM ELEMENT NO. 61101F; PROJECT NO. LDFP; TASK NO 07; WORK UNIT ACCESSION NO C7

11. TITLE (Include Security Classification)

ADVANCED GUIDED WAVE ELECTRO-OPTICAL SWITCHES

12. PERSONAL AUTHOR(S)
O. Eknoyan and H. F. Taylor

13a. TYPE OF REPORT	13b. TIME COVERED	14. DATE OF REPORT (Year, Month, Day)	15. PAGE COUNT
Final	FROM Apr 87 TO Apr 89	February 1990	52

16. SUPPLEMENTARY NOTATION
N/A

17. COSATI CODES			18. SUBJECT TERMS (Continue on reverse if necessary and identify by block number)
FIELD	GROUP	SUB-GROUP	Optical Waveguides Lithium Tantalate Electrooptic Switches
20	06		

19. ABSTRACT (Continue on reverse if necessary and identify by block number)

Efforts have concentrated on the use of LiTaO3 which is emerging as a superior alternative to the more commonly used LiNbO3 because of its higher immunity to optical damage. The progress made has resulted in the establishment of vapor diffusion technique for making low loss optical waveguides and its extension for making low loss waveguides by thermal diffusion below Curie temperature that support both TE and TM modes; the development of polarization independent guided-wave electrooptic switches; and the realization of lowest propagation loss ridge waveguides using the RIE process. Progress has also been made on the use of SBN:60. Specifically, a method for producing rib structures has been devised and high index optical waveguides have been obtained.

20. DISTRIBUTION/AVAILABILITY OF ABSTRACT ☒ UNCLASSIFIED/UNLIMITED ☐ SAME AS RPT ☐ DTIC USERS	21. ABSTRACT SECURITY CLASSIFICATION Unclassified
22a. NAME OF RESPONSIBLE INDIVIDUAL Richard A. Soref	22b. TELEPHONE (Include Area Code) (617) 377-2380 22c. OFFICE SYMBOL RADC (ESOC)

DD Form 1473, JUN 86 *Previous editions are obsolete.* SECURITY CLASSIFICATION OF THIS PAGE

UNCLASSIFIED

ADVANCED GUIDED WAVE ELECTRO-OPTICAL SWITCHES

Table of Contents

ADVANCED GUIDED WAVE ELECTRO-OPTICAL SWITCHES

Contract No. F19628-87-K-0027

I. SUMMARY

Several advances have been made on the use of lithium tantalate ($LiTaO_3$), a commercially available useful electrooptic material, which is emerging as a superior alternative to the more commonly used lithium niobate ($LiNbO_3$) due to its higher immunity to optical damage. The progress made includes: (1) the establishment of a vapor diffusion technique for making low loss optical waveguides, (2) the establishment of polarization independent guided-wave switches and modulators, (3) the extension of the vapor diffusion method for producing optical waveguides below the Curie temperature that support both TE and TM types of polarization, and (4) the realization of lowest propagation loss ridge waveguides by reactive ion etching (RIE). Progress has also been made on the use of strontium barium niobate (SBN:60) for applications toward the development of low voltage, wide angle, compact electrooptic crossbar switches. Specifically, a method for producing rib structures has been devised and high index optical waveguides have been obtained. Two (2) graduate students have contributed to these accomplishments which resulted in six (6) publications.

II. INTRODUCTION

Guided-wave electrooptic devices are needed for various applications in optical systems including navigation, sensing, computing, data transmission, and communications amongst others. A critical requirement for the functional operation of these devices hinges on the availability of single mode waveguides. Whereas their efficient performance necessitates the use of the largest possible electrooptic coefficient in available electrooptic materials. A cystal that has widely been used for this purpose is lithium niobate

($LiNbO_3$), and methods for producing single mode waveguides in it have been well established [1]. A primary reason for the concentration of efforts in this material stems from its relatively large Curie temperature, T_c~1170°C, value. This is higher than the temperatures encountered in the diffusion processes used for waveguide fabrication which typically range between 950 - 1125 °C [2]. As a result, the inherent electrooptic properties of the crystal are believed to remain intact, and the crystal stays poled. The largest electrooptic coefficient in $LiNbO_3$ is r_{33}, and to utilize it, electrodes in a guided-wave device fabrication are arranged so as to introduce an internal electric field that is oriented in the direction of the crystal optical axis. However, in spite of r_{33} being the largest in this material, geometrical restrictions limit interaction between electrical and optical fields and lead to the use of rather long waveguides in order to reduce electrical power drive. Furthermore, the relatively low optical damage threshold value of $LiNbO_3$ (~40 W/cm^2 at room temperature), is a major source of concern in the stability of devices produced in this material.

This work was initiated to explore the use of electrooptic materials other than $LiNbO_3$ that could offer large r_{33} electrooptic coefficient values. Attention was also focused towards the use of crystals that exhibit large optical damage threshold values and thus can withstand high levels of optical power. The ultimate goal was to produce novel guided-wave electrooptic switches. For these reasons, strontium barium niobate (SBN:60) was chosen due its large r_{33} value which is approximately fifteen (15) times that of $LiNbO_3$, and lithium tantalate ($LiTaO_3$) was selected due to its higher optical damage threshold value which is almost forty (40) times that of $LiNbO_3$. Table I lists some of these parameters which are later used as a basis for comparison between the three (3) mentioned electrooptic materials.

A detailed description of the results achieved on $LiTaO_3$ and SBN is given in the following section.

Table I. Selected properties of some electrooptic materials (all at wavelength of 0.633μm, except threshold at 0.515μm)

	$LiNbO_3$	$LiTaO_3$	SBN
T_c (°C)	~1175	~660	~75
n_e	2.2028	2.1833	2.2820
n_o	2.2866	2.1786	2.3177
$\lvert n_e - n_o \rvert$	0.0838	0.0046	0.0357
ε	28	43	880
r_{33} (x 10^{-12}m/V)	31	30	420
r_{51} (x 10^{-12}m/V)	28	20	13
Threshold (W/cm^2)	40	1500	*

* strong pyroelectric

III. RESULTS

Several advances have been made with the use of $LiTaO_3$ and SBN electrooptic crystals. These include the development of techniques t, produce low-loss optical waveguides, the realization of novel polarization independent switches and modulators, and the establishment of methods to produce rib structures. In the remainder of this section, details of the techniques and achieved results are presented.

III. a) Low-loss optical waveguides in lithium tantalate by vapor diffusion :

Optical waveguides in $LiTaO_3$ have commonly been produced by diffusing deposited films of transition metals at elevated temperatures. The choice of metal has often been Ti, and the diffusion process typically performed at temperatures in the range of 1150 - 1200 °C [3,4]. However at such high temperatures, special care must be taken to prevent outdiffusion of lithium which produces undesirable surface waveguides that compete with channel waveguides. Although methods for supressing outdiffusion have been reported [5], the task remains a formidable challenge. To overcome such difficulties, low temperature diffusion is desirable. This requires the use of elements that have high diffusivity and low activation energy, and that upon diffusion cause an index increase for both the ordinary and extraordinary modes of polarization. During the course of this work, Zn was found to be a suitable choice and its diffusion into $LiTaO_3$ was characterized. The diffusions were performed from the vapor phase and initially carried out at 800 °C which is significantly lower than that of Ti metal diffusion (~1200°C). Both planar and channel waveguides were produced. The former was used to characterize the vapor diffusion process of Zn into $LiTaO_3$, and the latter was developed to extend the technique for electrooptic devices fabrication. No outdiffusion was observed and the resultant waveguides were found to exhibit propagation losses that are

substantially below those obtained from Ti diffused ones.

The procedure for planar waveguide fabrication consisted of loading a cleaned bare 12.0x8.0x0.5 mm Y-cut $LiTaO_3$ sample together with ~12mm long 0.25 mm diameter Zn wire in a quartz ampule which was evacuated with a diffusion pump and sealed at a gauge pressure of about 10^{-7} Torr. The diffusion was performed by heating the ampule in a tube furnace. After completion of the diffusion, the ampule is pulled out and the substrate is removed. The substrate was observed to be dark gray at this step. To remove this discoloration, about 30 min annealing in an open tube furnace at 650 °C without any gas flow was followed. Waveguiding was observed for both TE and TM polarizations by end-fire coupling for propagation in the X-direction at 0.6328 μm. The Zn ion distribution in the diffused layer was chracterized on an angle-lapped sample using an electron microprobe [6]. The distribution was found to follow a complementary error function variation. This is expected since the diffusant Zn species may be considered an infinite source.

To characterize the effects of temperature and pressure, three identical Y-cut substrates were diffused for 6 h at three different temperatures -- 800, 850, and 900 °C. The substrates were obtained from a commercial supplier (Crystal Technology, Palo Alto, CA). The evacuated ampules were sealed to provide volumes of ~15 ml. This allows sustaining equilibrium vapor pressure for Zn at each of the noted temperatures. The resulting planar waveguides were then charcterized at λ = 0.6328 μm using a rutile prism coupler. The surface index change Δn and diffusion depth d were determined by fitting the measured effective indices of the supported modes of optical polarization to normalized universal dispersion charts [7]. From the measured d values, the Diffusion coefficient D was then evaluated using the relation $d = 2\sqrt{D\,t}$, where t is the diffusion time. The calculated D values were then used to determine the activation energy E_a and preexponential factor D^* from

$$D = D^{*}.\exp[-(E_a/kT)] \qquad (1)$$

where k is Boltzmann's constant and T is the absolute diffusion temperature. Fig. 1 shows the dependence of index change on temperature, for both ordinary and extraordinary modes, obtained after 6 h of diffusion in Y-cut substrates. The index change for a mode "i" is defined as the difference between the measured effective index of that mode $(n_{eff})_i$ and the bulk index n_b, viz., $\Delta n_i = (n_{eff})_i - n_b$. As the diffusion temperature was raised, the number of modes was observed to increase (Table II). The data presented in Fig. 1 correspond to the lowest order (fundamental) mode. Table II lists the number of modes observed for each polarization after 6 h of diffusion. The obtained index changes for the extraordinary mode were consistently larger than those from the ordinary mode (Fig. 1), and were typically observed to be more sensitive to variations in diffusion temperature and pressure. The equilibrium vapor pressure of Zn over the temperature range 800-900^{0}C is also shown in Fig. 1 (dashed line) [8] and it reflects the pressure that was generally maintained in the ampules during diffusion at the various temperatures.

Table II. Observed number of modes in Y-$LiTaO_3$ after 6-h diffusion.

T(^{0}C)	Zn mass (mg)	No. of modes TE	TM
800	16.02	1	1
850	16.40	2	1
900	15 83	2	2

Fig. 2 shows the dependence of diffusion coefficient D on diffusion temperature T for both the ordinary (TM) and extraordinary (TE) modes. For the examined temperature range they vary between 10^{-11} and 10^{-12}

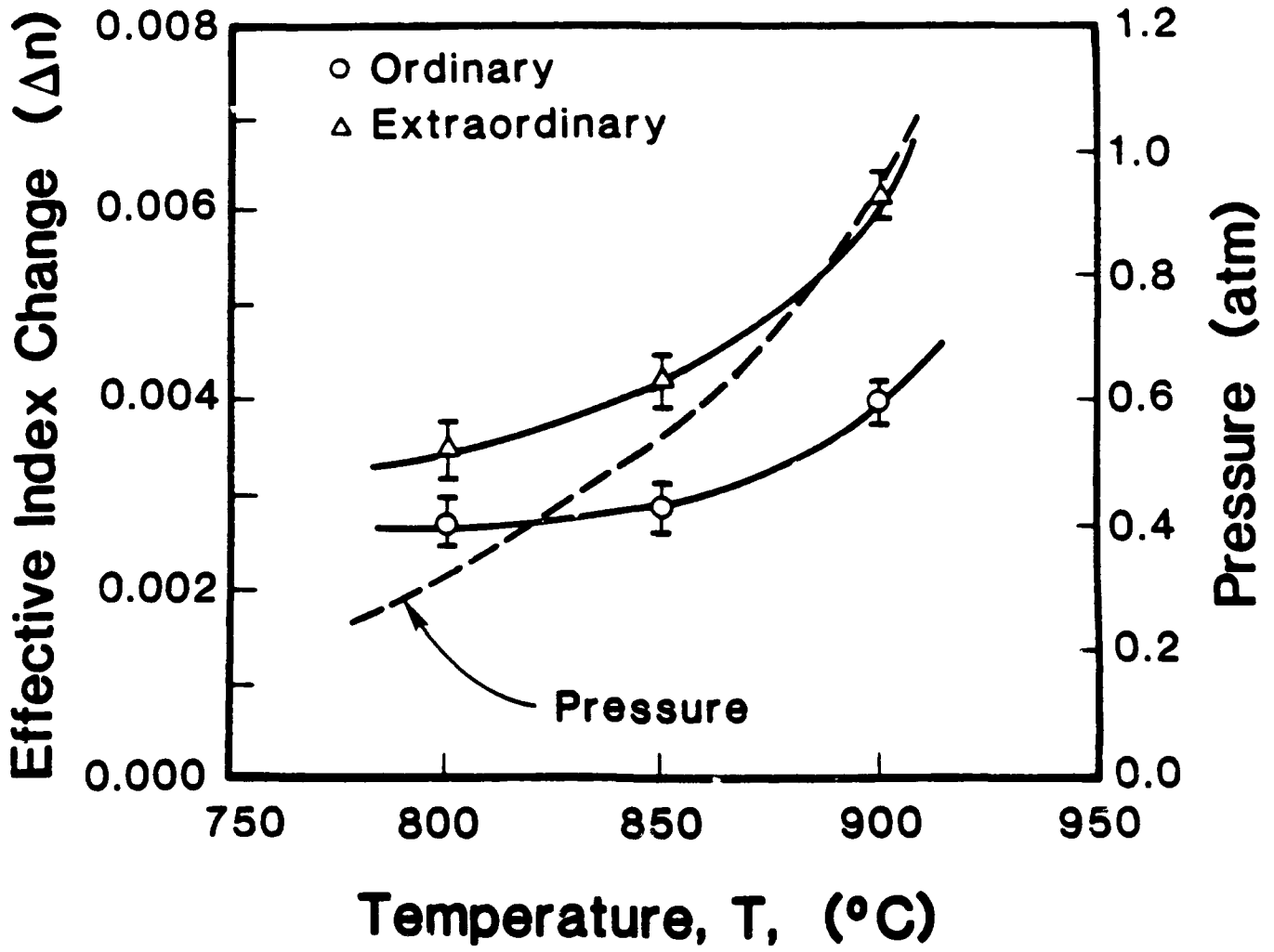

Fig. 1. Index change of fundamental modes (λ = 0.6328 μm) as a function of diffusion temperature in Y-$LiTaO_3$ after 6 h. The Dashed line represents equilibrium vapor pressure for Zr at various temperatures.

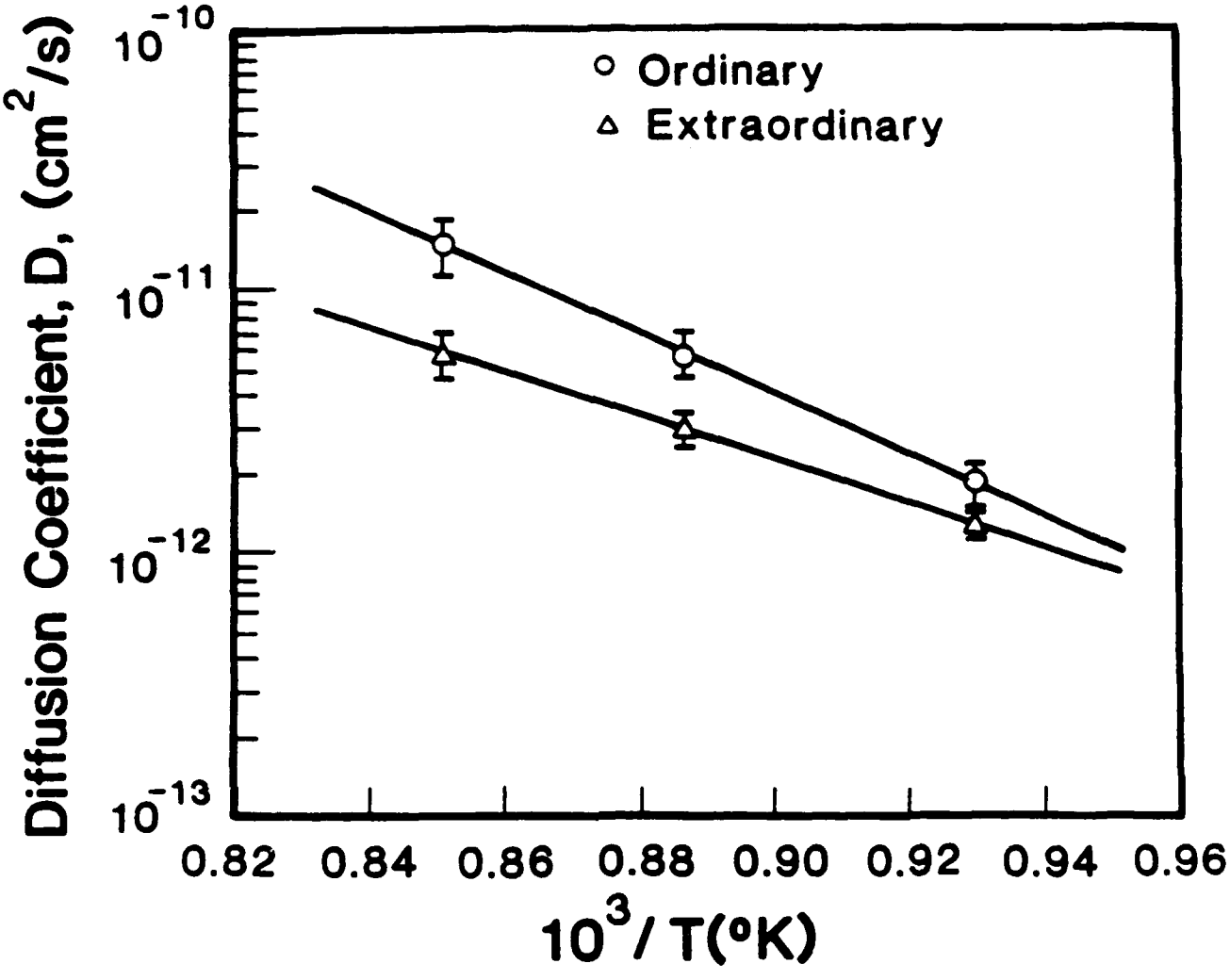

Fig. 2. Diffusion coefficient dependence on temperature for Zn diffused into Y-$LiTaO_3$.

cm^2/s. The diffusion coefficient value obtained at 800 °C comparable to that reported for Ti diffusion into $LiTaO_3$ at 1200°C [3]. This is indicative of the high diffusivity of Zn into $LiTaO_3$, which makes it useful for low temperature diffusion. Low temperature diffusion is desirable to reduce outdifussion. The diffusion coefficient for outdiffused layers in $LiTaO_3$ normal to the optical C-axis is less than 10^{-11} cm^2/s (~ $2x10^{-12}$) at 800°C, and equals $9x10^{-10}$ cm^{-2}/s (~ 10^{-9}) at 1200°C [9]. This large difference, which is roughly three orders of magnitude, slows outdiffusion to such an extent that any index change which it produces is extremely small to allow outdiffused surface waveguiding. This was experimentally verified by heating a bare sample in an evacuated ampule without Zn for 6 h at 800°C and not observing any waveguiding for either mode afterward [6]. These observations indicate that in $LiTaO_3$: (1) outdiffusion effects on index change are negligible at these low temperatures, and (2) Zn diffusion was necessary for waveguide formation. The calculated values of the activation energy E_a and preexponential factor D^* were 1.69 eV and 5.29 x $10^{-5}cm^2/s$ for the extraordinary mode, and 2.21 eV and 3.85 x 10^{-2} cm^2/s for the ordinary mode. To characterize diffusion time effects, the substrates were placed back in ampules and diffused longer, with the same amount of Zn that was used initially included in the new ampules. The measured effective diffusion depths d are plotted against $\sqrt{t}$ in Fig. 3. The non-zero intercepts at t = 0 h correspond to diffusion that has occured during the ampule's insertion into the furnace and before reaching the actual diffusion temperature. The ampules were inserted slowly (~ 4 cm/min) into the furnace to avoid thermal shock to the crystals. Accompanying the increase in diffusion depth, larger values for the effective index changes were obtained for both types of polarization with the additional diffusion times.

The results described thus far were all obtained on Y-cut substrates. Diffusion experiments at 800°C for 600 h were also carried out on X-, and Z-cut substrates. Both cuts produced effective

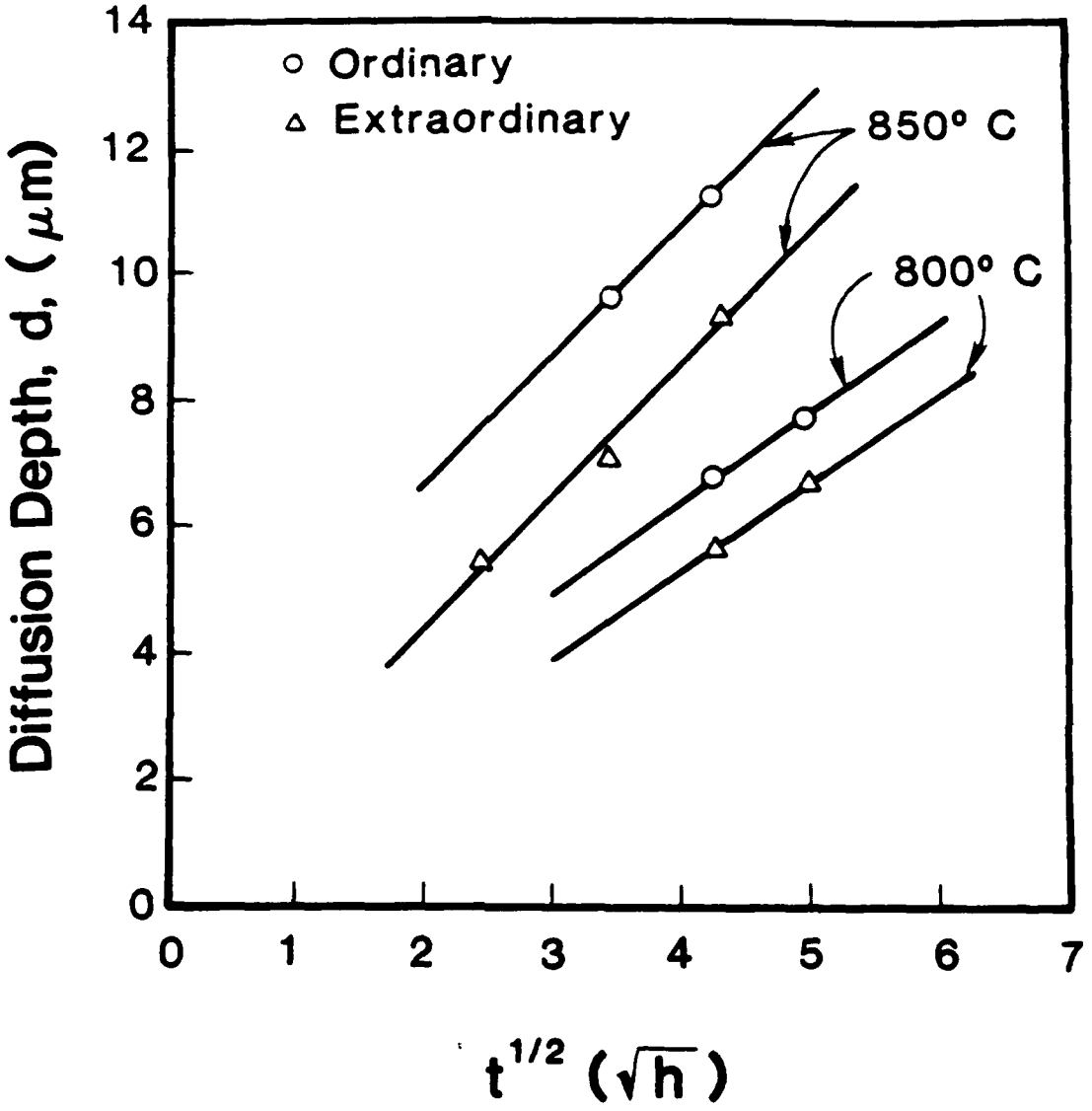

Fig. 3. Variations of measured effective diffusion depth d with time (as $\sqrt{t}$) at various temperatures for Zn into Y-$LiTaO_3$.

index changes of ~0.002 and ~0.004 for the ordinary and extraordinary modes, respetively. However, the X-cut substrates exhibited single mode for both polarizations, whereas the Z-cut substrates produced two modes for the extraordinary (TM) polarization and only one mode for the ordinary (TE) polarization. Addditional experiments were performed to determine the effect of pressure on X- and Z-cut substrates at 800°C by varying the amount of Zn. No significant variations were seen for the effective index change. However a slightly decreasing trend for the surface index change was observed in the double moded (extraordinary polarization) Z-cut substrates as summarized in Table III. Comparable data were of course, unobtainable for the single-mode X-cut substrates since they supported only one mode.

Table III. Vapor pressure, ammount of Zn, and surface index change for the extraordinary mode in Z-cut $LiTaO_3$ after 6 h at 800°C diffusion.

P (atm)	Zn mass (mg)	$(n_s - n_b)$
0.101	1.20	0.00769
0.200	2.40	0.00898
0.305	5.25	0.00920
0.305	16.40	0.00961
0.305	39.23	0.01079

Channel waveguides were also produced by the vapor diffusion method on Y-cut $LiTaO_3$ substrates and were used for propagation loss measurements. These were obtained by etching through a 4000 Å sputtered SiO_2 mask, photolithographically delineated channel patterns prior to loading in an ampule for diffusion. The Zn diffusion was carried out at 800°C for 6 h. Following similar preparation

procedures as those described above for the slow push-in and pull-out of ampule, oxidation, and polishing, the substrates were tested for optical guiding by end fire coupling at 0.6328 μm wavelength. No outdiffused mode propagation was observed between the channels. This is attributed to the low diffusion temperature used and partially to the presence of the SiO_2 masking film on the substrate surface that may have acted as a cap in supressing LiO_2 outdiffusion. Measurements on a 5 μm wide channel waveguide in a 12 mm long sample showed propagation losses of 3.0 dB/cm before poling and 0.8 dB/cm after poling, for the TE polarization. The overall insertion loss of 4.6 dB for the poled sample included 1.3 dB losses introduced by the input and output objectives, 1.3 dB Fresnel losses, ~1.0 dB coupling mismatch loss, and an additional attenuation of 1.0 dB for propagation losses along the waveguide length. The larger value obtained before poling may be due to scaterring from inversion centers formed during diffusion above the crystal Curie temperature, and also possibly from the sputtered SiO_2 film which was initially left on the substrate but removed after poling. The attenuation figures of these vapor diffused waveguides are well below those obtained by the commonly used method of Ti indiffusion. A value of ~4.7±1.0 dB/cm was measured on channel waveguides produced for comparison by 270Å Ti diffusion at 1150°C, in X-cut $LiTaO_3$ substrates after poling [6]. The poling was performed by cooling diffused substrates through the $LiTaO_3$ Curie temperature, from 730 to 500 °C, under a 167 V/cm electric field applied along the crystal axis across Pt electrodes.

To verify the effectiveness of poling, modulation experiments were successfully demonstrated on a Mach-Zehnder type interferometer. The device exhibited an extinction ratio of 30 dB (99.9% modulation depth) at 4.5 volt V_π value.

III. b) Optical waveguides in $LiTaO_3$ by vapor diffusion below Curie temperature :

Despite the abundant availability of both lithium-niobate and

-tantalate crystals commercially, no extensive use has been made in the past of $LiTaO_3$ primarily due to its low Curie temperature (T_c ~510-690°C depending on composition). This makes repoling of crystals a necessity for producing electrooptical devices when waveguides are formed by diffusion at a temperature higher than T_c. Attempts to fabricate waveguides below Curie temperature have been reported. These include ion-,proton-exchange [10,11], and electrodiffusion [12]. However in the ion and proton exchange methods, an index increase is observed only for the extraordinary mode, while in the field assisted diffusion the limitation is prompted by strong absorption peaks and surface damage.

On the basis of this work finding Zn to be a fast diffusant in $LiTaO_3$, it was decided to use the Zn vapor diffusion approach for producing waveguides in this crystal below its Curie temperature. The fabrication process is similar to that described earlier. Initially, a cleaned substrate was loaded together with Zn into a quartz ampule which was evacuated and sealed. The ampule was then heated to 595°C in a tube furnace for several hours. This temperature is below the 615°C Curie point of the commercially obtained Y-cut crystals. After 115 h of diffusion, the ampule was removed from the furnace and broken to remove the substrate, which was then cleaned and polished along its edges. Waveguiding was observed for both TE and TM polarizations at 0.6328 μm. Better waveguides were obtained however after 240 h of diffusion. To verify that Zn caused waveguides formation, the described procedure was repeated without Zn in a sealed ampule containing a similar crystal. No waveguiding was observed in such a sample. Optical mode measurements with a rutile prism coupler revealed effective index changes of ~0.002 and 0.001 for the fundamental TE and TM polarization modes, respectively. Propagation loss measurements were also performed on these waveguides using the test arrengement shown in Fig.4. The cylindrical lens was used to optimize matching between the coupled light field distribution and guided mode profile. The mode size was established in an end fire coupling setup by translating an avalanche photodetector that was

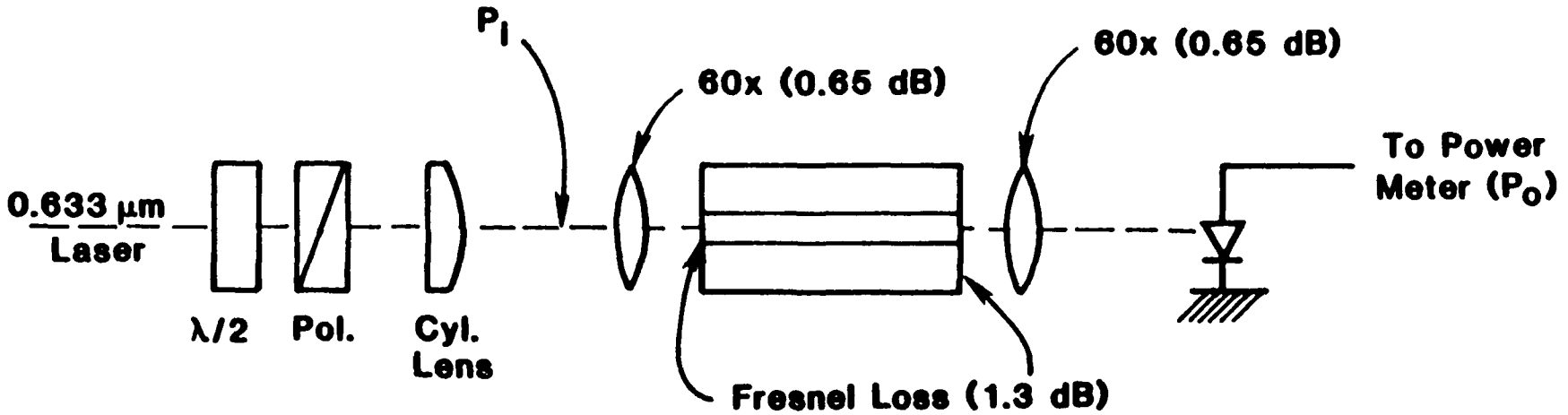

Fig. 4. Experimental arrangement for propagation loss measurement.

mounted on a translation stage, lateraly side ways, until 1/e value of the peak power was reached. Table IV summarizes the results. Attenuation figures of 2.5 and 4.0 dB/cm were obtained for the TE and TM modes of polarization respectively, in a 4 μm wide channel waveguide produced by a 595°C/115h diffusion. The table also shows that mode mismatch losses for this waveguide were ~0.7 dB for TE and ~1.0 dB for TM. Near field patterns for the same waveguide are shown in Fig. 5.

To verify that the electrooptic properties of the crystal were maintained intact, modulation experiments were demonstrated at 0.6328 μm wavelength for both modes of polarization on interferometers produced by 595°C/115h diffusion without repoling. The interferometer was a symmetric Mach-Zehnder type modulator, Fig. 6, which had a total branching angle of 2°, electrode length of 4 mm/arm, a channel width of 4 μm, and electrode gap of 8 μm. The electrodes were delineated in a 2000 Å aluminum film. The modulator performance for a TE polarized input in a Y-cut $LiTaO_3$ substrate is shown in Fig. 7. This particular device exhibited an extinction ratio of 30 dB (~99.9% modulation depth) and a π-radian voltage of 6.4 V, correponding to a value of 0.3 for the electrical/optical fields overlap.

III. C) Enhancement of refractive index by combining metal and vapor diffusion :

Controlled variation in the refractive index of waveguides is desirable for many electrooptical devices. Techniques to obtain such changes for waveguides produced in $LiNbO_3$ and glass have been reported by several workers and for diferrent needs. However most of these approaches required tight control of fabrication parameters and are difficult to produce. Means for controlling variations in the index change of optical waveguides produced in $LiTaO_3$ are also needed. A relatively simple technique to provide such controls has been established during the course of this work [13]. The procedure

	Pol.	Insertion loss(dB)	Mode mismatch (dB)	PROPAGATION LOSS(dB/cm)
with cyl. lens	TE	6.0	0.82	2.45
	TM	7.4	0.6	4.03
without	TE	6.7	1.5	2.45
	TM	8.4	1.6	4.03

Table IV. Summary of loss measurements on a 4 μm channel waveguide produced by Zn vapor diffusion.

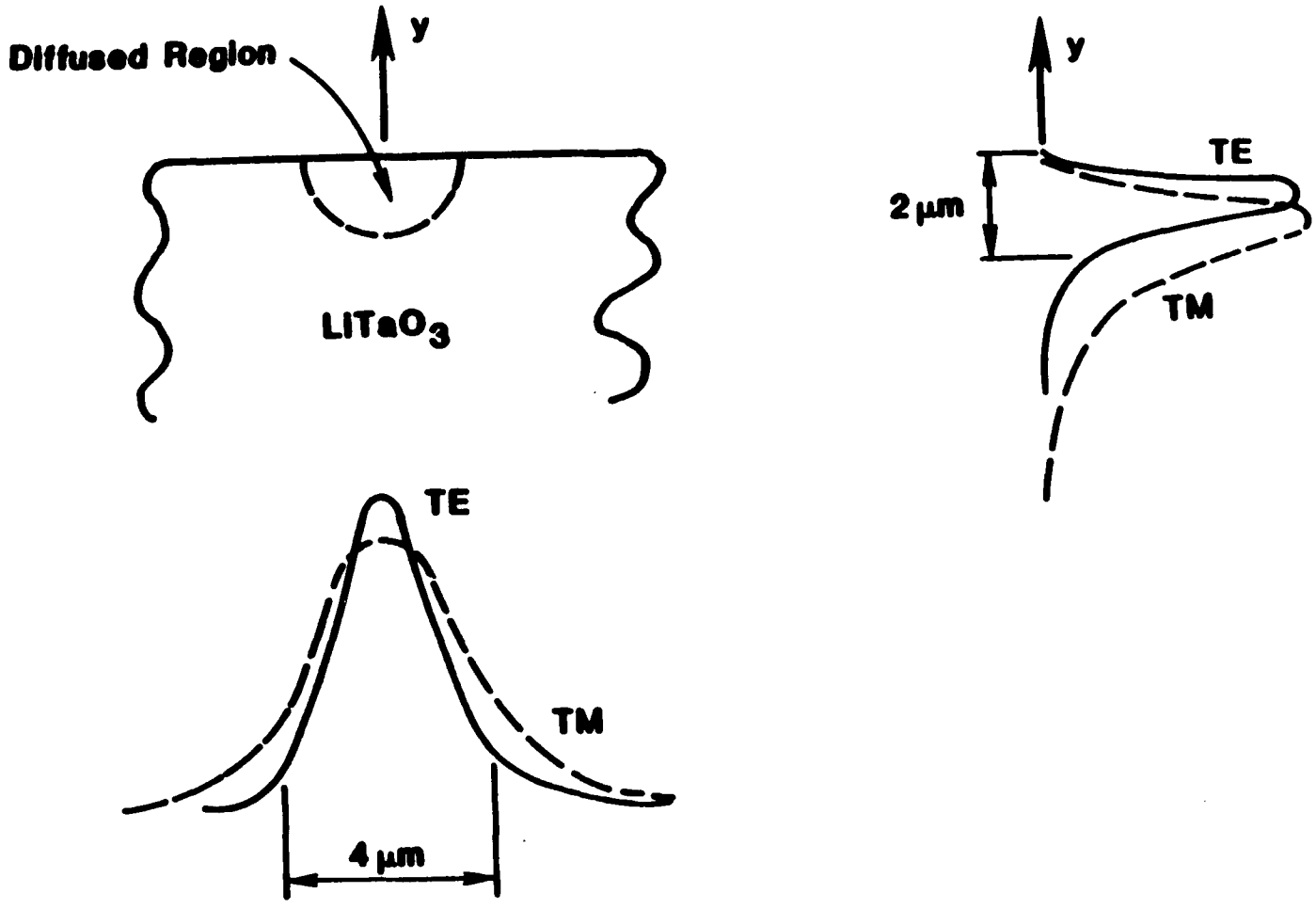

Fig. 5. Near field patterns for TE and TM modes of polarization in a 4 μm channel waveguide produced by a 595°C/115h Zn vapor diffusion.

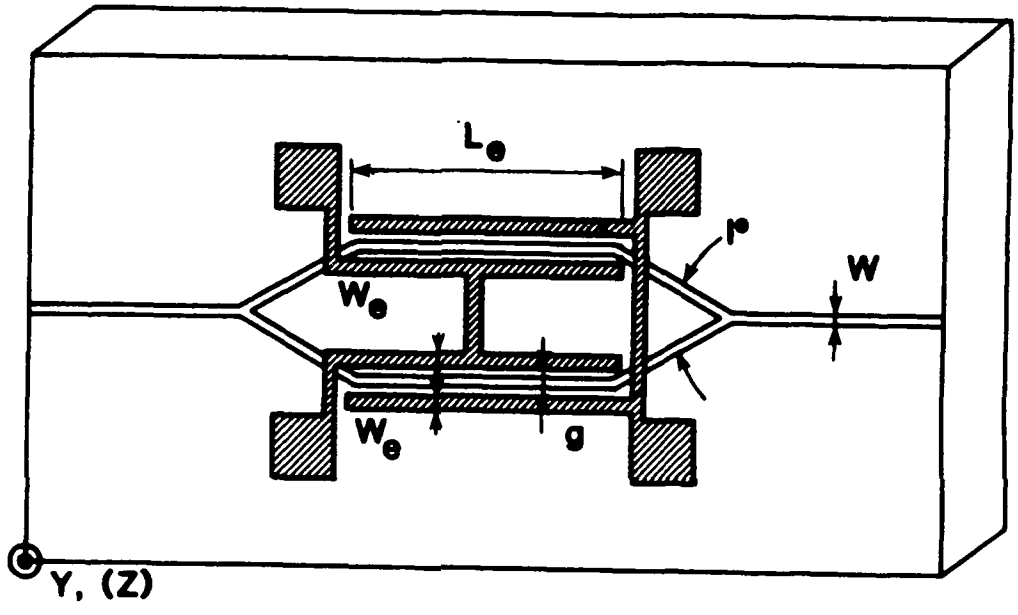

$L_e = 4mm$ $W_e = 10\ \mu m$

$W = 4\ \mu m$ $g = 8\ \mu m$

Fig. 6. Schematic representation of modulator structure.

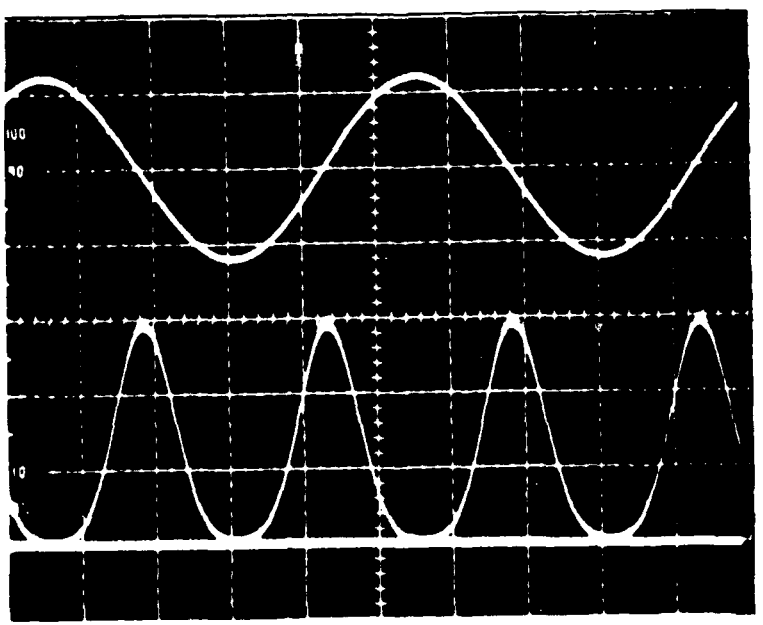

Electrical (5V/div)

Optical (5mV/div)

Fig. 7. Typical performance of a modulator produced without repoling of Y-$LiTaO_3$ crystal after diffusion.

involved the application of a vapor diffusion technique in a double diffusion process to enhance the effective index of optical planar waveguides initially produced by Ti indifussion. In the second diffusion step, Zn is introduced from the gaseous phase at such low temperatures that the additional increase in effective indexes is achieved without noticeably affecting the depth of the initial waveguides.

Table V summarizes the parameters for the initial Ti diffusion that was carried out on two X-cut and one Z-cut substrates, listing film thickness "τ", and diffusion temperature "T" and time "t" (columns 3, 4, and 5).

Table V. Diffusion conditions for Ti and Zn, with corresponding waveguides depth (X and Z designate substrate cuts, subscripts refer to extraordinary and ordinary polarization)

Sample		Ti Diffusion				Zn diffusion		
		τ(Å)	T(°C)	t(h)	d(μm)	T(°C)	t(h)	d(μm)
X4	e	335	1150	14	2.83	800	6	4.02
	o				2.64			4.24
X5	e	290	1200	9	2.85	750	9	3.03
	o				2.65			3.15
Z5	e	290	1200	9	4.20	750	9	3.50
	o				3.36			2.85

The sputter deposited films were oxidized at 650°C for 4 h in dry O_2 ambient prior to diffusion. All diffusions were then performed in quartz furnace tubing in a lithium vapor ambient with ~1.2 l/min flowing O_2. The resulting planar waveguides were characterized by a calibrated rutile prism at 0.6328 μm wavelength. The calculated effective index value for the fundamental mode n_{eff}(Ti) for each

sample, and their corresponding surface index change $\Delta n_s(Ti)$ and diffusion depth d as obtained from universal dispersion curves for a Gaussian index profile are listed in columns 3 and 4 of table VI and column 6 of table V, respectively. The procedure for the second (vapor) diffusion step is identical to that described in sections III.a (p. 4) and III.b (p. 12). The temperature and time of this diffusion are listed in table V (columns 7 and 8). After performing the Zn diffusion, the samples were reoxidized at 650°C for 20 min in an air ambient. Prism measurements at 0.6328 μm were repeated. Refractive index values higher than those of the initial Ti indiffused waveguides were consistently obtained and generally without a change in the number of observed modes. The measured effective index values of the fundamental modes after the second diffusion, $n_{eff}(Zn+Ti)$, and the amount of their increase above those obtained initially from Ti indiffusion δn are listed in column 6 and 8 of Table VI.

To estimate expected effective index changes after double diffusion, the WKB method [14] for a graded index distribution was used. An index distribution for the waveguide of the form

$$n(y) = n_b + \Delta n_T \exp\left[- (y/d_T)^2 \right] + \Delta n_Z \operatorname{erfc} (y/d_Z) \qquad (2)$$

was assumed. In this equation n_b is the refractive index of the bulk substrate, Δn_T and Δn_Z are the surface refractive index increase for Ti and Zn diffusions respectively, d_T and d_Z are their corresponding diffusion depths, and y is the depth beneath the surface of substrate. The above relation assumes Gaussian distribution for Ti indiffusion, and complementary error function distribution for the Zn vapor diffusion. Calculation of effective indices n_{eff} for the guided modes is based upon numerical eigenvalue solutions to the scalar wave equation

$$\frac{d^2u}{dy^2} + k_0\left(n^2(y) - n_{eff}^2 \right) u = 0 \qquad (3)$$

Table VI. Surface and effective index changes for Ti and Ti/Zn diffusion, and index enhancement δn of the fundamental mode (subscripts refer to extraordinary and ordinary polarization).

Sample		Δn_s(Ti)	n_{eff}(Ti)	Δn_s(Zn)	n_{eff}(Ti+Zn)		δn
					Measured	Calculated	measured
X4	e	0.0174	2.1944	0.0086	2.1999	2.2005	0.0055
	o	0.0106	2.1841	0.0038	2.1868	2.1868	0.0027
X5	e	0.0164	2.1936	0.0056	2.1968	2.1971	0.0032
	o	0.011	2.1845	0.0036	2.1864	2.1866	0.0019
Z5	e	0.0122	2.1916	0.00537	2.1947	2.1950	0.0031
	o	0.01	2.1855	0.00324	2.1865	2.1867	0.001

with $k_0 = 2\pi/\lambda$, subject to the boundary conditions $u(0) = 0$, $u(y) \sim e^{-\alpha y}$, $y \to \infty$, with $\alpha = k_0(n_{eff}^2 - n_b^2)^{1/2}$.

To substantiate this model, the index distribution given above was used to perform numerical calculations for the fundamental mode (m = 0) case with n_b = 2.1833 and 2.1786 for the extraordinery and ordinary polarizations, respectively. The measured surface index change and diffusion depth value of Ti indiffusion were used for Δn_T and d_T. For the Zn case on the other hand, values measured after Zn vapor diffusion in bare $LiTaO_3$ substrates and listed in column 5 of table VI under Δn_s(Zn), also the last column of table V under d(μm) were used respectively for Δn_Z and d_Z appearing in (2). The results obtained from calculations are listed for comparison in table VI next to the measured effective index values. The agreement between the two is within 10^{-4}. Using the data obtained for the fundamental mode in the initial Ti diffusion step, normalized parameters

$$V = k_o d\ (n_s^2 - n_b^2)^{1/2} \qquad (4)$$

and

$$b = (n_{eff}^2 - n_b^2) \ / \ (n_s^2 - n_b^2) \qquad (5)$$

were calculated. The results are plotted in Fig. 8, and agree well with those predicted for the fundamental mode from an assumed Gaussian index distribution [3]. For comparison, normalized index b values calculated by using the surface index increase of Ti only, and n_{eff}(Ti + Zn) data obtained from both experimental measurements and model predictions are also shown on the figure. Although the b values obtained by using n_s(Ti) after double diffusion are not exact, they nevertheless show graphically the increase in effective indexes relative to the initial values obtained after Ti diffusion only. The increase in the effective indexes listed under δn in Table VI are accurate, as they are obtained from fundamental mode angles and make no use of surface index values. The good agreement achieved between model predictions and experimental results further confirm their accuracy.

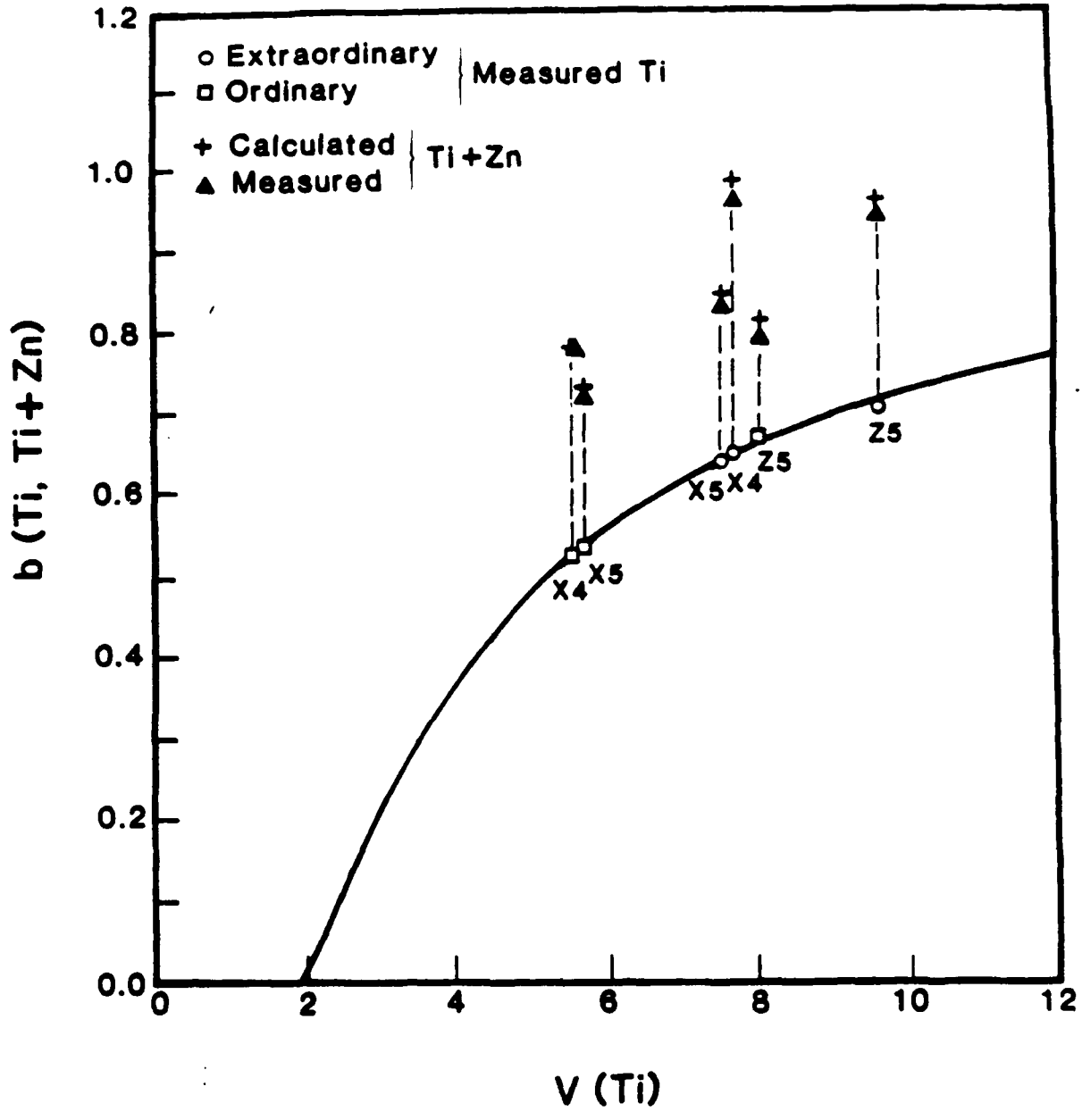

Fig. 8. Normalized mode dispersion (solid curve) for the fundamental mode of a planar waveguide obtained from a Gaussian index distribution.

III. d) Polarization independent guided-wave switches and modulators :

Since the polarization of light transmitted through typical fiber optic systems flactuates randomly between two orthogonal states [15], guided-wave electrooptic devices that are independent of polarization are needed for use at the terminals of such systems. All of the efforts for producing such devices however have concentrated on the use of $LiNbO_3$ as a substrate material, and have mostly been directed towards the fabrication of directional coupler type switching devices [16-18] that utilize the relatively weak r_{13} electrooptic coefficient. Accordingly, the voltage-length (VL) product of these devices has been high due to its inverse dependence on the electrooptic coefficient. Futhermore, only one attempt has been made for producing a polarization independent interferometric type modulator [19], but two independent voltages were required for its operation. This device was also produced in $LiNbO_3$ and involved the use of r_{13}, r_{33}, and r_{22} electrooptic coefficients. To overcome these limitations, polarization independent switches and modulators that are based on the concept of TE-TM mode coupling via the off-diagonal r_{51} electrooptic coefficient [20] have been developed in $LiTaO_3$ [21,22]. The choice of this material was prompted primarily by its low birefringence $|n_o - n_e|$ value relative to $LiNbO_3$. This permits an increase in device optical bandwidth, and also allows a longer spatial period for the electrodes that are needed for attaining the required phase matching between the two (TE and TM) orthogonal states. Furthermore by using r_{51}, lower values for the (VL) product can be anticipated. Material parameters listed in Table I (p. 3) provide a basis for making a comparison between $LiTaO_3$ and $LiNbO_3$ as a substrate choice for these devices.

A schematic of the developed polarization independent switch structure, illustrating substrate orientation and electrode pattern is shown in Fig. 9. Under this arrangement in birefringent $LiTaO_3$, the TE and TM modes couple through the off-diagonal r_{51} electrooptic coefficient via an x-directed electric field component. Assuming that the TE and TM polarization modes are (1) phase matched, (2) have equal

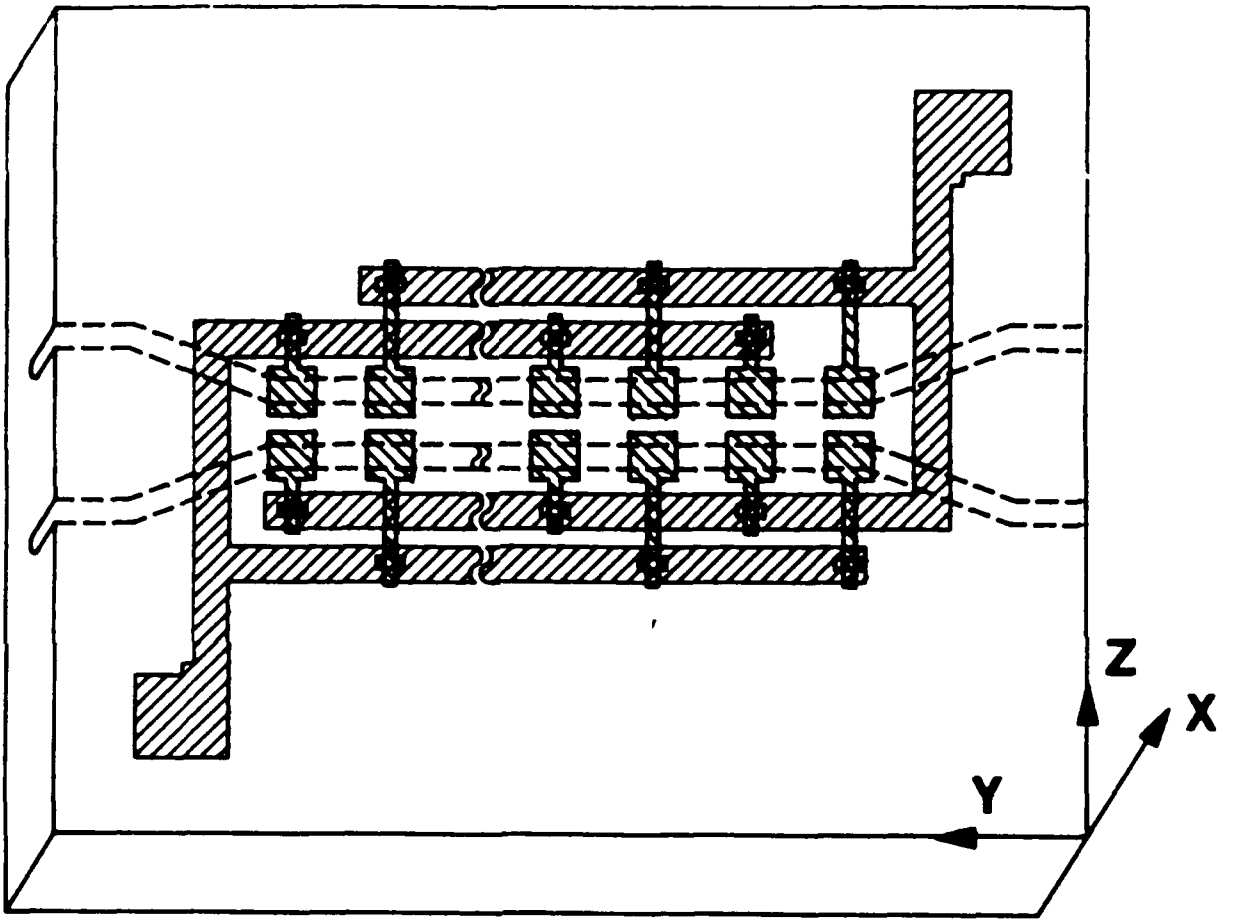

Fig. 9. Schematic representation of device structure for a polarization independent switch.

interguide coupling coefficient κ, and (3) exhibit identical field amplitude profiles, the electrooptically induced index change can be expressed as

$$\Delta n = \frac{n^3}{2} \; r_{51} \; E. \qquad (6)$$

Here, n is the index of refraction, and E is the electric field given by E = V/g with g being the electrode separation and V the applied voltage. The phase matching is achieved when the condition

$$\frac{2\pi}{\lambda_o} \; | \; n_{TE} - n_{TM} | \; = \frac{2\pi}{\Lambda} \qquad (7)$$

is satisfied, where n_{TE} and n_{TM} are the effective indices of the fundamental modes for TE and TM polarizations, λ_o is the free space wavelength of the optical signal, and Λ is the spatial period of the electrodes. Using the minimum index change requirement for switching $\Delta n . (L/\lambda) = \sqrt{3} \; / \; 4$, and combining with the above realtion results in

$$V.L = \frac{\sqrt{3} \; \lambda \; g}{2 \; n^3 \; \alpha \; r_{51}} \; . \qquad (8)$$

Here L is the interaction length, and the factor α is a constant determined by the overlap between optical and applied electric fields.

Optical channel waveguides for the symmetric directional coupler (Fig. 7) of ~3 μm width were produced by Zn vapor diffusion into x-$LiTaO_3$ with z perpandicular to the channels. The diffusion was performed at 800°C for 6 h following procedures described earlier in section III.a (p. 4). For operation at 0.6328 μm wavelength, the length of the channels, L, along their parallel interaction region were chosen to vary between 2.1 and 3.9 mm. Substrates were then edge polished and poled. Aluminum electrodes ~2000 Å thick were next

delineated on top of a thin (~1200 Å) SiO_2 buffer layer to produce devices of Λ = 112, 124, and 140 μm with different number of repeated N periods. These spacings were determined from eq.(7) using birfringence valus of 0.0045-0.0057 that were measured initially with a prism coupler on planar waveguides at 0.6328 μm. A 5000 Å thick SiO_2 insulating film was later deposited on top of the electrodes, and vias were opened through it to provide external connection to the buried lower level electrodes. Finally a second 2000 Å Al layer was evaporated on the surface and patterned to produce the electrode interconnection desired for the application of the periodic electric field perturbation, as shown in Fig. 7.

The coupling characteristics of the parallel waveguides were tested by end fire coupling. The interguide transfer efficiency η of directional couplers having various interaction lengths was determined as a function of separation from the ratio

$$\eta = \frac{P_1}{P_1 + P_2} \qquad (9)$$

where P_1 and P_2 are measured output powers in the cross and bar states respectively. Using the measured values of η and the relation

$$\eta = \sin^2 (\kappa L + 2\phi) \qquad (10)$$

where 2ϕ represents finite coupling in the bent regions of the waveguides, the coupling coefficient κ was determined. The transfer length $\ell = \pi/2\kappa$, was then caculated using these values for κ. The results are shown graphically versus measured interguide separation d^* in Figure 10, where d^* is the measured waveguides separation obtained after etching.

The completed devices were tested for switching and modulation at 0.6328 μm. Initial testing revealed that the channel waveguide birefringence differed slightly from that measured on planar

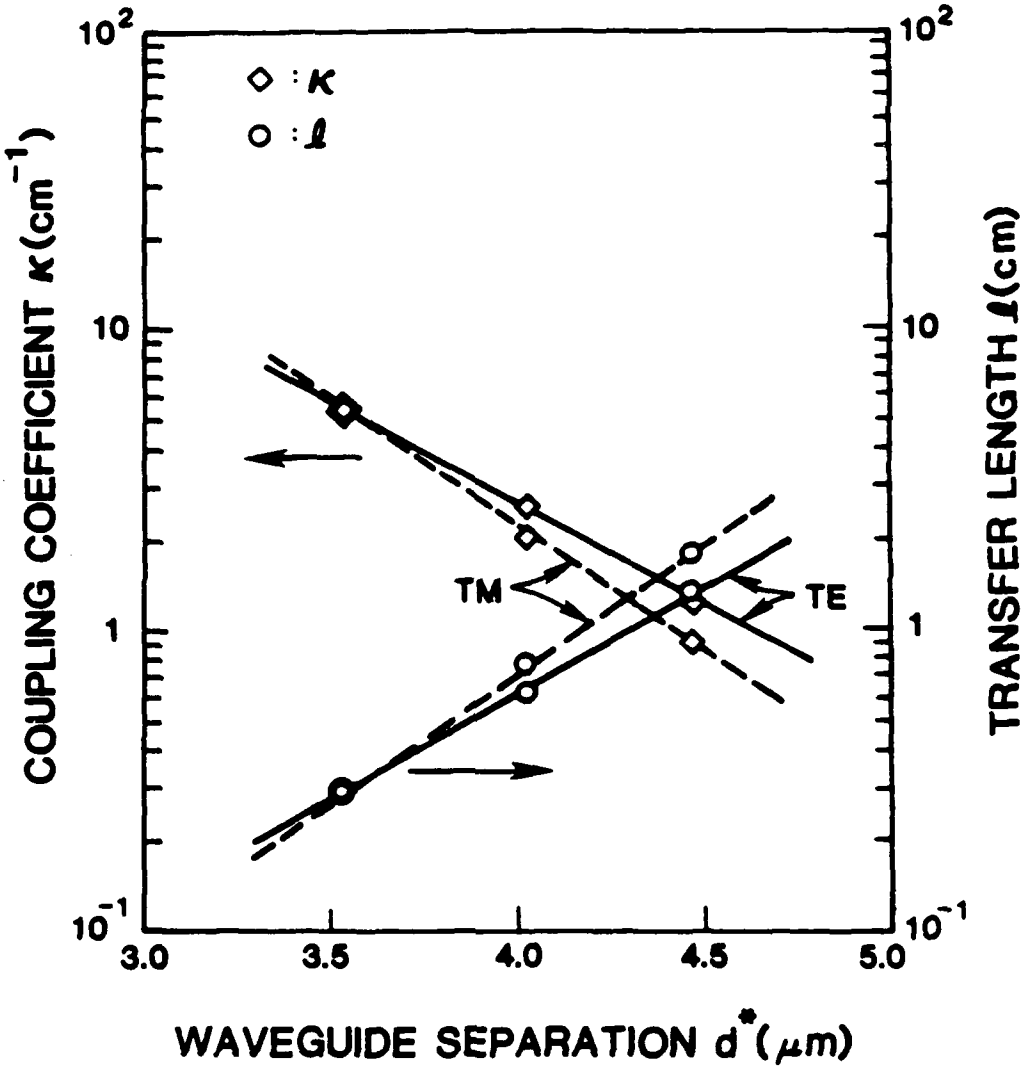

Fig. 10. Coupling coefficient κ and transfer length ℓ versus measured interguide separation d^*.

waveguides and used as a basis in determining the periodicity of electrodes. This is expected by virtue of the dimensional confinement in channels geometry and was likely intensified by the SiO_2 loading effect. To compensate for this, the temperature dependence of the birefringence in $LiTaO_3$ was used to adjust the phase match point. This was done by placing the substrate on a temperature controlled thermoelectric stage and thermally tuning for maximum modulation. Typical measurement data for the temperature effect on a device having N = 24, Λ = 140 μm tuned at 18.5°C are shown in Fig. 9 (circles), and are in good agreement with the expected behavior (solid line) abtained from the relation

$$\eta = \frac{\kappa^2}{\kappa^2 + \delta^2} \sin^2 \sqrt{\kappa^2 + \delta^2} \cdot L \qquad (11)$$

where κ is the coupling coefficient, and $\delta = \Delta\beta/2$ is a measure of the mismatch between the propagation constants in the two orthogonal modes which can be thermally adjusted. Figures 11 (a) and (b) show the modulation performance of a switch (S11 in table VII) for both TM and TE polarizations. Modulation testing results for other selected devices are summarized in VII and reveal maximum attained switching efficiencies of 99.8% for TM and 95% for TE at nearly equal externally applied voltages.

Table VII. Summary of slected device* performance

Device	L (cm)	Λ (μm)	T_o (°C)	η (%) TM	η (%) TE	V.L (V-cm) TM	V.L (V-cm) TE
S4	0.210	140	10.9	95.0	91.0	30.97	34.86
S11	0.211	124	20.0	99.8	95.0	33.44	29.96
S18	0.213	112	27.5	88.8	89.1	33.86	33.87

* All devices had channel width of 3.5μm

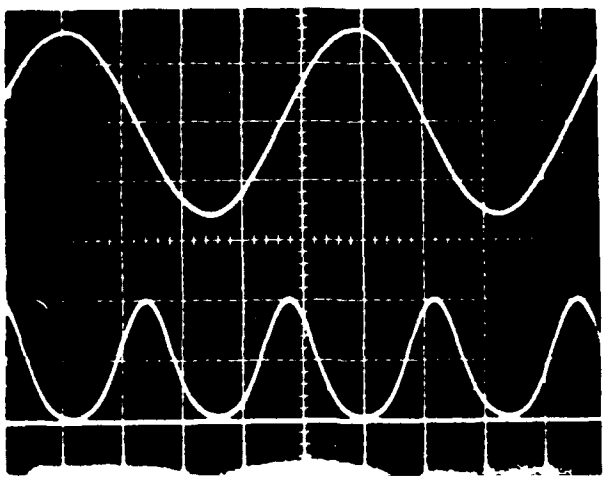

(a)

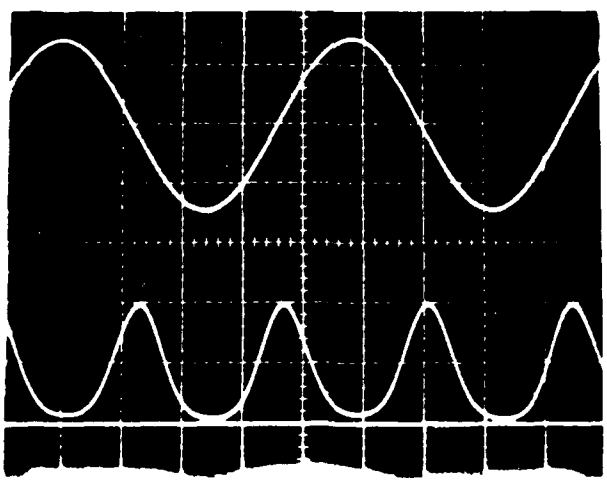

(b)

Fig. 11. Modulation performance of a polarization independent switch (device S11) (a) TM, (b) TE; for each frame upper trace is electrical signal (100 V/div), lower trace is optical output (20 mV/div), f=10 kHz.

Figure 12 is a schematic drawing for an interferometric polarization independent guided-wave electrooptic modulator that was also produced in $LiTaO_3$, as an extension of the same concept that was utilized in the development of the switches described above. The final devices required thermal tuning for optimum operation. Tables VIII and IX summarize device parameters and behavior for a selected number of tested modulators. All devices were produced by 800°C 6 h Zn-vapor diffusion on X-cut substrates, and had 3.92 mm inteaction length/arm.

Table VIII. Device parameters of polarization independent modulators

Device	g (μm)	Λ (μm)	N (periods)	transverse modes number TE	TM
D4	4	112	35	2	1
D5	4	140	28	1	1

Table IX. Summary of modulation test results

Device	T_o (°C)	VL (V-cm)	modulation depth TE	TM
D4	26	17.64	80	80
D5	21	23.52	85	85

The large voltage length product values attained in both switches and modulators is due to a weak overlap between electrical and optical fields. These can be improved by a tighter control in photolithography.

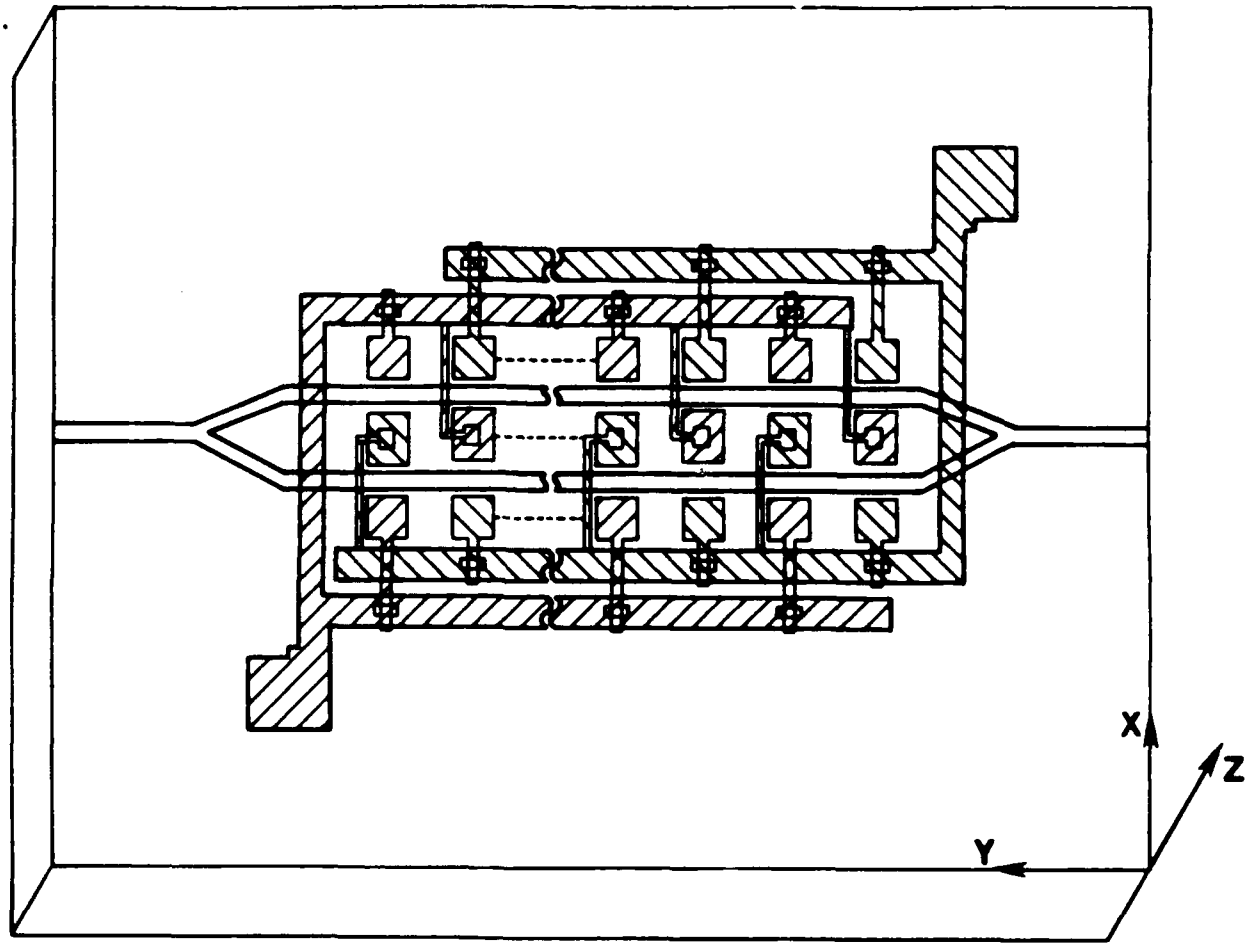

Fig. 12. Schematic drawing of device structure for polarization independent Mach-Zehnder interferometric modulator.

III. e) Rib waveguides :

Most guided-wave electrooptic devices are produced using the planar technology. Channel waveguides formed by this technique are imbedded within the bulk of crystal adjacent to its surface, and usually exhibit good guiding characteristics. However, the small index change encountered across their lateral sides ($n_g - n_s$), where n_g is the waveguide effective index and n_s is the substrate refractive index, has limited channels bending to less than ~1.5° so as to minimize the radiation losses [23]. To overcome this limitation, the use of rib waveguides becomes necessary. In such structures the lateral index change increases, as it becomes measured relative to air instead of substrate. This allows a tighter confinement of the optical field and thus permits larger bending. The interest for developing rib waveguides in this work was prompted by their suitablity for making large angle crossbar switches. Device considerations indicates that wide crossing angle and low voltage switches could best be realized through the use crystals with large electrooptic coefficients. For this reason, strontium barium niobate (SBN:60) was identified as a viable alternative to the more commonly used and commercially available $LiNbO_3$. The electrooptic coefficient r_{33} of SBN is approximately twelve (12) times that of either $LiNbO_3$ or $LiTaO_3$ (Table I, p. 3). However due to the scarcity of SBN crystals, the develoment of rib structure has been optimized on Zn diffused $LiTaO_3$ substrates. The process has also been successfully extended to SBN and preliminary results have been obtained.

III. e(1) Rib Waveguides in $LiTaO_3$:

The rib waveguides were produced by reactive ion etching (RIE) technique on Zn diffused Z-cut $LiTaO_3$. The Zn was diffused from vapor phase at 800°C for 6 h following procedures described in section III-a. The substrate's end faces parallel to the optical Z-axis, were then polished. Using a liftoff technique, straight line metal patterns to provide a protective mask during etching were delineated

perpendicular to the polished end edges (Z-axis). The patterned lines varied in width between 1.0 to 10.0 μm in increments of one micron. Various types of metal films were used for masking. Best results were obtained with sputtered Ni:Cr (80:20) alloy, and e-beam deposited Ni films. In each case, the films were deposited on top of a thin (~80 Å) Cr layer to insure good adhesion. However due to anisotropy in sputtering deposition, an undesirable thin metal film was always found to exist after liftoff on the surface of substrates adjacent to the side walls of the thick masking lines. These side films were eliminated when an e-beam technique was used, apparently due to more directional uniformity of deposition by this method. All the ribs were formed by RIE process in a commercial Drytek DRIE-100 system. The system had an aluminum chamber, operated at 13.56 MHz, and was adjusted to provide 6.35 cm separation between square shaped electrode plates of 17.8 cm/side. RIE is widely used in semiconductor based technology, and its use in etching undiffused $LiNbO_3$ has been reported but without examining the optical guiding behavior of the resultant structures [24]. For etching Zn:$LiTaO_3$ in this case, several gas mixtures, pressures, and power levels were attempted. Best results were obtained using 3:3:3 SCCM flow rate of CCl_2F_2:Ar:O_2, in a 5 μm pressure and at 350 watts. Under these conditions, clean smooth surfaces were realized with etching rates selectivity of 1:65 Å/min between the NiCr mask and $LiTaO_3$ substrate, and 1:58 Å/min in the case of Ni/$LiTaO_3$ masking arrangement. Figure 13 is a scanning electron micrograph of a 4.0 μm wide, 0.5 μm high ridge structure produced with a Ni mask.

Optical characterization was performed at 0.6328 μm wavelength by end fire coupling from a He:Ne laser. Figure 14 shows horizontally scanned near field pattern profiles for TE and TM input polarizations obtained on a 6 μm wide, 2.7 μm high, 11.7 mm long rib waveguide produced on Z-$LiTaO_3$ substrate. The strong mode confinement in the lateral direction, corresponding to air/waveguide/air, is clearly evident for both polarizations. A vertical scan near field pattern is shown in Fig. 15. Propagation loss measurements were also performed

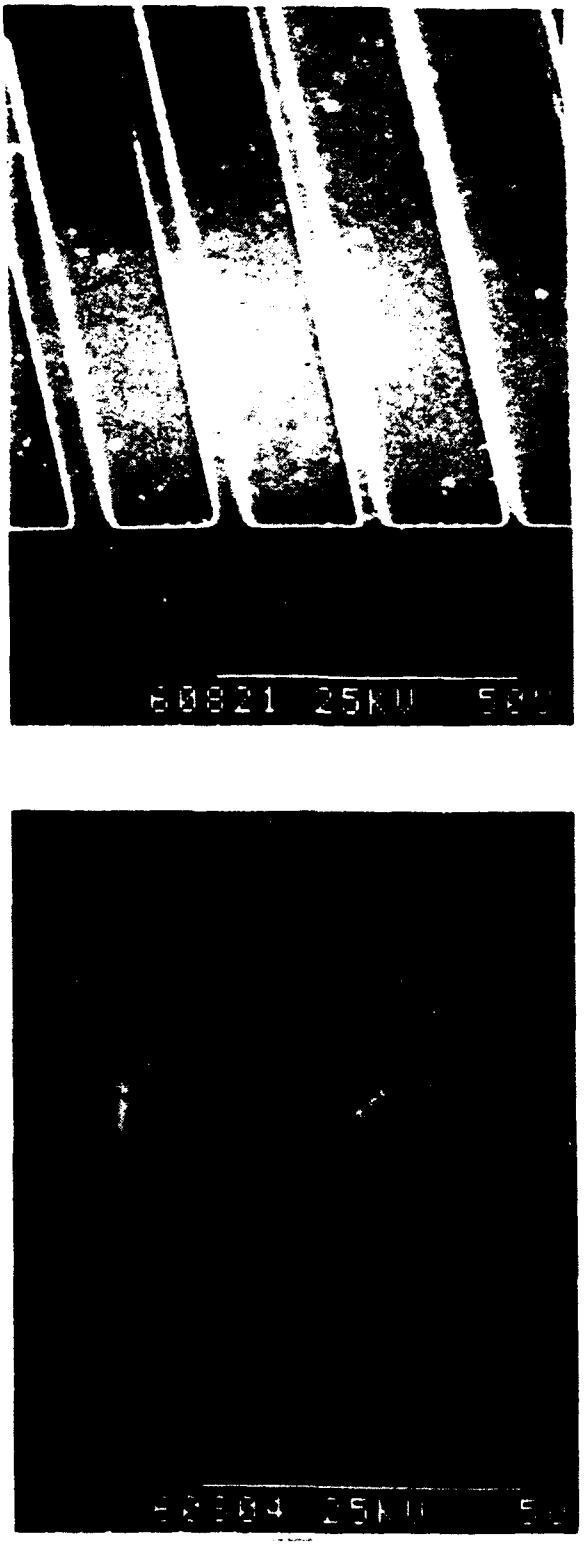

Fig. 13. SEM micrograph of rib structures produced on SBN crystal by reactive ion etching.

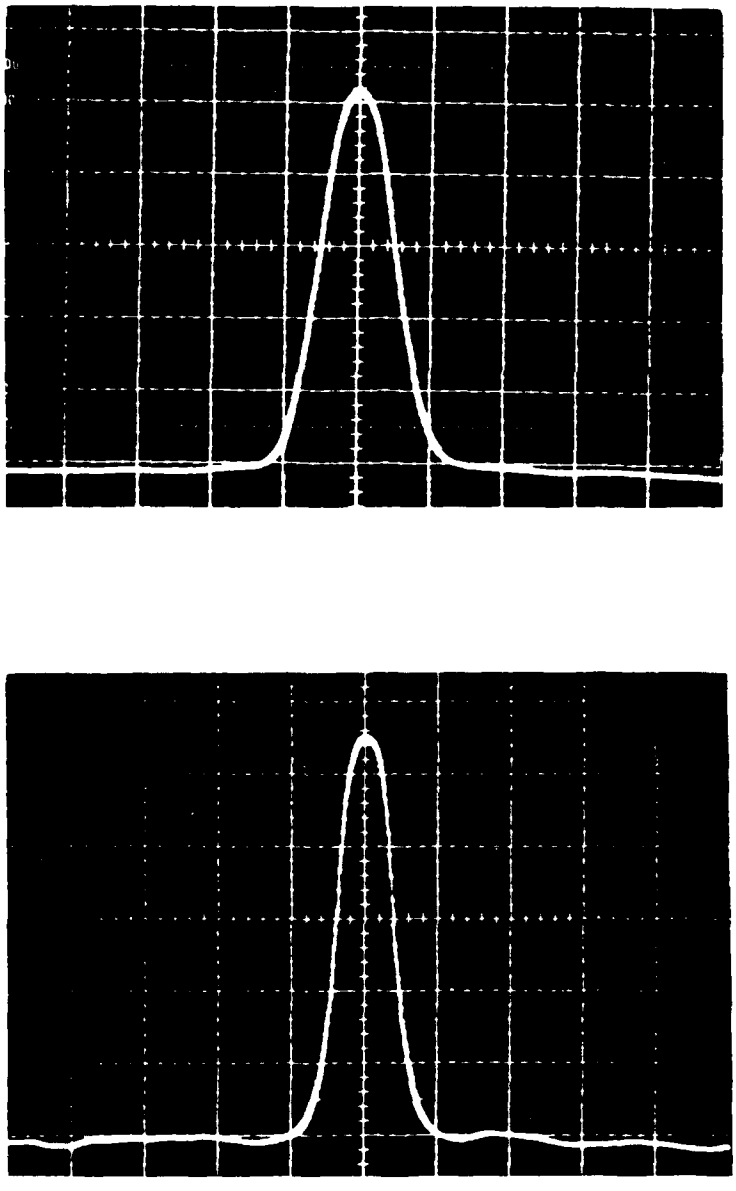

Fig. 14. Near field patterns obtained by a horizontal scan of the output from a Zn-$LiTaO_3$ 2.7 μm high rib waveguide for (a) TE, (b) TM input polarizations (λ=0.6328 μm).

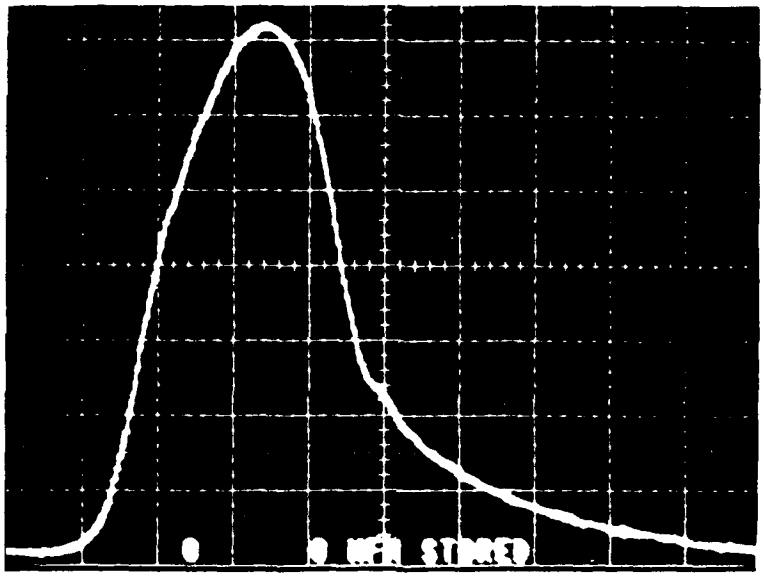

Fig. 15. Near field pattern obtained by a vertical scan of the output from a Zn-$LiTaO_3$ 2.7 μm high rib waveguide for a TE input polarization (λ=0.6328 μm).

on rib waveguides of different heights. The results are listed in Table X. The 2.35 dB/cm attenuation figure is the lowest ever acheived for rib waveguides in any ferroelectric crystal. The larger losses measured for the higher rib structures must clearly be associated with strong scattering from rough walls on the rib sides. This roughness is beleived to be formed by uneven edges (thickness and shape) of the metal mask lines, that are initiated during phtolithography and then further intensified during etching. Another difficulty that also resulted from photlithography was prompted by the thicker resist which forms near the sharp edges of the crystal after spinning. This produces significant variation in the width uniformity of the patterned metal mask lines, and contributes to additional losses in the final rib waveguides. Ridge waveguides have previously been produced in Cu diffused $LiTaO_3$ by sputter etching [25]. However no attenuation figures were reported for that case.

Table X. Propagation losses in X-cut Zn:$LiTaO_3$ rib waguides produced by RIE

Mask metal	Rib height (μm)	Propagation loss (dB/cm) TE	TM
Ni/Cr	0.50	6.77	2.35
Ni:Cr/Cr	1.76	8.65	11.69
Ni:Cr/Cr	2.70	10.29	12.11

III. e(2) Rib waveguides in SBN:60 :

Two SBN:60 samples, each 18 mm in diameter, were supplied by R.R. Neurgaonkar of Rockwell International Science Center for this work. One of these has been used for developing an etch process for SBN, and also in exploring means for making waveguides by methods other than S diffusion [26]. Progress was made in each case, but further investigations are needed.

The RIE process developed for the Zn:$LiTaO_3$ was found to also be suitable in etching SBN. Using 80:20 Ni:Cr alloy metal for masking, an etch rate selectivity of 8:63 Å/min between the metal mask and undiffused SBN substrate was achieved in CCl_2F_2:Ar:O_2 gas mixture with flow rates, pressure, and rf power identical to those given in III.e(1) for $LiTaO_3$. Optical testing however was not performed, since the substrate was not diffused initially and was too little in size to be polished.

In the search for alternatives to S that might be used as diffusant to form high index guiding regions, Zn was found to offer a possible choice. Planar and channel waveguides that support the extraordinary (TM) mode of polarization were produced using Zn diffusion from vapor phase at 800°C into Z-cut SBN. Prism coupling attempts at 0.6328 μm wavelength on planar waveguides diffused for 6 h and annealed for 30 min at 650°C revealed a continium of modes that could not be well differentiated. At least 5 modes were estimated to exist. An effective index change of approximately 0.02 with corresponding diffusion length of ~7 μm were calculated. Propagation loss measurements performed at 0.6328 μm on a 4 mm long, 6 μm wide channel waveguide produced attenuation figures ranging from ~30 dB/cm after a 30 min anneal time, to ~16 dB/cm after 14 h of annealing. These figures were obtained from insertion loss measurements by applying corrections of 1.3 dB for the input and output objectives loss, 1.3 dB for Fresnel losses, and 0.9 dB for the coupling mismatch loss. The channel waveguides were produced by diffusing through photolithographically delineated patterns etched in a 4000 Å thick SiO_2 surface masking film. Strong guiding of the extraordinary (TM) mode of polarization was also observed at 0.82 μm wavelength. Efforts are currently continuing to produce a Mach-Zehnder interferometric modulator on the second of two supplied SBN substrates. Very low modulation voltage is expected for the final devices.

III. f) Publications from contract:

1. O. Eknoyan, D.W. Yoon, and H.F. Taylor, "Low-Loss Optical Waveguides in Lithium Tantalate by Vapor Diffusion," *Appl. Phys. Lett.*, vol. 51, p. 384, August 1987.

2. D.W. Yoon and O. Eknoyan, "Characterization of Vapor Diffused Zn:LiTaO3 Optical Waveguides," *IEEE J. Lightwave Technology*, vol. 6, p.877, June 1988.

3. H.S. Jung, O. Eknoyan, and H.F. Taylor, "Enhancement of Refractive Index in LiTaO3 Optical Waveguides," *IEEE J. Lightwave Technolgy*, vol. 7, p. 370, Dec. 1989.

4. D.W. Yoon, O. Eknoyan, and H.S. Jung, "Optical Waveguides in Lithium Tantalate by Vapor Diffusion Below Curie Temperature," OSA-IEEE/IGWO '88, Santa Fe, N.M., March 1988.

5. D.W. Yoon, O. Eknoyan, and H.F. Taylor, "Polarization Independent LiTaO3 Guided Wave Electrooptic Switches," *IEEE J. Lightwave Technology*, to be published in January 1990.

6. H.S. Jung, H.F. Taylor, and O. Eknoyan, "Interferometric Polarization Independent Waveguide Modulators in LiTaO3," *IEEE J. Lightwave Technology*, accepted for publication.

IV. REFERENCES

1. R.C. Alferness, "Waveguide electrooptic modulators," *IEEE Trans. Microwave Theory Tech.*, vol. MTT-30, p.1121, Aug. 1982.

2. G.J. Griffith and R.J. Esdaile, "Analysis of Titanium diffused planar optical waveguides in lithium niobate," *IEEE J. Quantum Electron.*, vol. QE-20, p.149, Feb. 1984.

3. W.K. Burns, P.H. Klein, E.J. West, and L.E. Plew, "Ti diffused in $LiNbO_3$ planar and channel waveguides," *J. Appl. Phys.*, vol. 50, p. 6175, Oct. 1979.

4. O. Eknoyan, W.K. Burns, R.P. Moeller and N.J. Frigo, "Broadband $LiTaO_3$ guided-wave TE-TM mode convertor," *Appl. Opt.*, vol. 27, p. 114, Jan. 1988.

5. B. Chen and A.C. Pastor, "Elimination of LiO_2 outdiffusion waveguide in $LiNbO_3$ and $LiTaO_3$," *Appl. Phys. Lett.*, vol. 30, p. 570, June 1970.

6. O. Eknoyan, D.W. Yoon, and H.F. Taylor, "Low-loss optical waveguides in lithium tantalate by vapor diffusion," *Appl. Phys. Lett.*, vol. 51, p. 384, Aug. 1987.

7. G.B. Hocker and W.K. Burns, "Modes in diffused optical waveguides of arbitrary index profile," *IEEE J. Quantum Electron.*, vol. QE-11, p. 270, June 1988.

8. R.C. Weast and M.J. Astle, Eds.,*CRC Handbook of Chemistry and Physics*, 60th ed. Boca Raton, FL: CRC, 1980, p. D-218.

9. J.R. Carruthers, I.P. Kaminow, and L.W. Stulz, "Diffusion kineticks and optical waveguiding properties of outdiffused layers in lithium niobate and lithium tantalate," *Appl. Opt.*,

vol. 13, p. 2333, Oct. 1974.

10. J. Jackel, "Optical waveguides in $LiTaO_3$: silver lithuim ion exchange," *Appl. Opt.*, vol. 19, p. 1996, June 1980.

11. W.B. Spillman, Jr., N.A. Sanford, and R.A. Soref, "Optical waveguides in $LiTaO_3$ formed by proton exchange," *Opt. Lett.*, vol. 8, p. 497, Sept. 1983.

12. J. Noda, T. Saku, and N. Uchida, "Fabrication of optical waveguides in $LiTaO_3$ by Cu diffusion," *Appl. Phys. Lett.*, vol. 25, p. 308, Sept. 1974.

13. H.S. Jung, O. Eknoyan, and H.F. Taylor, "Enhancement of refractive index in Ti:$LiTaO_3$ optical waveguides by Zn vapor diffusion," *J. Lightwave Technol.*, vol. 7, p.390, Feb. 1989.

14. R.H. Dicke and J.P. Wittke, *Introduction to Quantum Mechanics.* Reading, MA: Addison-Wesley, 1960, p. 245.

15. R.A. Steinberg and T.G. Gialloernzi, "Performance limitations imposed on the optical waveguide switches and modulators by polarization," *Appl. Opt.*, vol. 15, p. 2440, Oct. 1976.

16. R.C. Alferness, "Polarization-independent optical directional switching using weighted coupling," *Appl. Phys. Lett.*, vol. 35, p. 748, Nov. 1979.

17. O.G. Ramer, C. Moh, and J. Pikulski, "Polarization-independent optical switch with multiple sections of $\Delta\beta$ reversal and Gaussian-taper functions," *IEEE J. Quantum Electron.*, vol. QE-18, p. 1772, Oct. 1982.

18. L. McCaughan, "Low-loss polarization-independent electrooptical switches in $\lambda = 1.3$ μm," *J. Lightwave Technol.*, vol. LT-2, p. 51, Feb. 1984.

19. W.K. Burns, T.G. Giallorenzi, R.P. Moeller, and E.J. West, "Interferometric waveguide modulation with polarization-idependent operation," *Appl. Phys. Lett.*, vol. 33, p. 944, Dec. 1978.

20. H.F. Taylor, "Polarization independent guded-wave optical modulators and switches," *J. Lightwave Technol.*, vol. LT-3, p. 1277, Dec. 1985.

21. D.W. Yoon, O. Eknoyan, anf H.F. Taylor, "Polarization independent $LiTaO_3$ guided-wave electrooptic switch," *J. Lightwave Technol.*, - in press.

22. H.S. Jung, H.F. Taylor, and O. Eknoyan, "Interferometric polarization independent waveguide modulator in $LiTaO_3$," *J. Lightwave Technol.*, - in press.

23. H.F. Taylor, "Power loss at directional change in dielectric waveguides," *Appl. Opt.*, vol. 13, p. 642, March 1972.

24. J.L. Jackel, R.E. Howard, E.L. Hu, and S.P. Lyman, "Reactive ion etching of $LiNbO_3$," *Appl. Phys. Lett.*, vol. 38, p. 907, June 1981.

25. J. Noda, N. Uchida, M. Minakata, T. Saku, and Y. Ohmachi, "Electro -optic intensity modulation in $LiTaO_3$ ridge waveguides," *Appl. Phys. Lett.*, vol. 26, p. 298, March 1975.

26. O. Eknoyan, C.H. Bulmer, H.F. Taylor, W.K. Burns, A.S. Greenblatt, L.A. Beach, and R.R. Neurgaonkar, "Vapor diffused optical waveguides in strontium barium niobate (SBN:60)," *Appl. Phys. Lett.*, vol. 48, p. 13, Jan. 1986.

MISSION
of
Rome Air Development Center

RADC plans and executes research, development, test and selected acquisition programs in support of Command, Control, Communications and Intelligence (C^3I) activities. Technical and engineering support within areas of competence is provided to ESD Program Offices (POs) and other ESD elements to perform effective acquisition of C^3I systems. The areas of technical competence include communications, command and control, battle management information processing, surveillance sensors, intelligence data collection and handling, solid state sciences, electromagnetics, and propagation, and electronic reliability/maintainability and compatibility.